

1 **Characterization of Seismicity from Different Glacial Bed Types: Machine Learning**
2 **Classification of Laboratory Stick-Slip Acoustic Emissions**

3 **S. Saltiel¹, N. Groebner², T. Sawi³, C. McCarthy³, B.K. Holtzman³**

4 ¹Nevada Seismological Laboratory, University of Nevada, Reno, NV, USA

5 ²Strabo Analytics, Inc, New York, NY, USA.

6 ³Lamont-Doherty Earth Observatory, Columbia University of New York, NY, USA

7 Corresponding author: Seth Saltiel (ssaltiel@unr.edu)

8 **Key Points:**

- 9 • Ice slip on frozen till or rock at high velocity produce stick-slip stress-drops with AEs
10 recorded on transducers frozen into the ice
- 11 • Supervised machine learning can determine bed type (rock versus frozen till) from
12 waveform or spectral features
- 13 • Feature importance shows till events are more impulsive/higher frequency, consistent
14 with higher stress-drops, friction, and healing

15 **Abstract**

16 Subglacial seismicity provides the opportunity to monitor inaccessible glacial beds at the
17 epicentral location and time. Glaciers can be underlain by rock or till, which determines the
18 mechanics of slip and, if unstable, characteristics of resulting seismicity. Utilizing a double direct
19 shear apparatus, we found conditions for instability at freezing temperatures and high slip rates for
20 both bed types, although with very different frictional evolution. During stick-slip stress-drops, we
21 recorded acoustic emissions with piezoelectric transducers frozen into the ice. Supervised machine
22 learning can classify recorded waveforms and spectra as coming from rock or till beds. The
23 Random Forest Classifier is interpretable, with the prediction based on the initial oscillation peaks
24 and high frequency energy. Till events are generally higher stress-drop, with more impulsive first
25 arrivals compared to rock waveforms. These seismic signatures of mechanical slip processes and
26 associated bed conditions can potentially greatly enhance interpretation of subglacial seismic data.

27 **Plain Language Summary**

28 A glacier can lurch forward while slipping on its base, releasing seismic waves like an earthquake,
29 which are monitored from the surface. Just like in a tectonic setting, only certain conditions allow
30 for this type of motion, and aspects of the bed conditions affect how they slip and the resulting
31 waves. We approximate glacial bed conditions in the lab of two very different types, soft
32 (sediment) and hard (rock), and measure lurching behavior and resulting waves from each. Using
33 a variety of data science techniques, we decipher subtle differences between the two bed types
34 from remotely-sensed waves. This suggests that seismicity can provide important information on
35 glacial bed conditions and how they differ in time and space.

36 **1 Introduction**

37 Future sea-level rise will largely be determined by fast-slipping polar glaciers, known as ice
38 streams [Cuffey & Paterson 2010]. Since motion is mostly concentrated at their beds, conditions
39 there have an outsized effect on the entire system's mass-balance and evolution. Glacial beds are
40 separated, to first order, into hard bedrock or soft sediment (till), and then as either 'wet' (melting
41 temperature) or 'dry' (frozen or drained) [Clarke 2005]. Water and sediment can flow and evolve
42 on much shorter time scales than ice deforms, so the bed is one of the most dynamic parts of the
43 ice sheet system, assumed to be responsible for recent changes in ice flow configurations
44 [Bougamont et al., 2015] and ongoing responses to the changing climate [Parizek et al., 2013].

45 Although the basal system is difficult to directly access, growing observations of subglacial
46 seismicity offer the opportunity to monitor changes with high temporal and spatial resolution
47 [Aster & Winberry 2017]. Recent studies have used subglacial seismicity observations to infer
48 differences in bed strength [Guerin et al., 2021], failure mechanism [Kufner et al., 2021], fine-
49 scale asperity interactions [Gräff et al., 2021], basal water pressure [Gräff & Walter 2021], as well
50 as local basal shear-stresses and slip-rates [Hudson et al., 2022].

51 Seismic observations are particularly useful since there are limited glacial bed conditions that have
52 been shown to exhibit the requisite conditions for seismic failure [Iverson 2010, Lipovsky et al.,
53 2019]. Classically, ice deformation, and thus slip due to regelation and viscous creep, is assumed
54 to be rate-strengthening [Schoof 2005]. Till deformation was also first treated as viscous but later
55 shown to be Coulomb plastic, essentially rate-neutral [Iverson 2010, Zoet & Iverson 2020]. But
56 nucleation of seismic instability requires rate-weakening resistance, described by the rate-state
57 stability parameter ($b - a$), which allows acceleration due to feedback with decreasing friction, as

58 has been shown for fault rocks and gouge [Marone 1998]. This situation provides the opportunity
59 for seismic observations to present a strong constraint on the conditions at their epicentral location
60 and origin time, but each potential stick-slip mechanism and characteristics of resulting seismicity
61 must be thoroughly understood to determine what conditions recorded seismic events represent.

62 Laboratory simulations provide the opportunity to directly observe slip behavior under controlled
63 conditions. To date, seismically required rate-weakening has been reported for debris-laden ice on
64 impermeable rock at sub-freezing temperature and permeable rock at the pressure melting point
65 [Zoet et al., 2013], pure ice on impermeable rock at sub-freezing temperature [McCarthy et al.,
66 2017], and pure ice on till at sub-freezing temperature [Saltiel et al., 2021], with stick-slip stress-
67 drops reported for debris-laden ice on impermeable rock at sub-freezing temperature [Zoet et al.,
68 2020]. These findings suggest that seismicity is largely associated with dry (frozen or drained)
69 conditions. Although fast-slipping glaciers are commonly assumed to occur on wet, temperate
70 beds, local mechanisms could freeze bed regions, for example around obstacles [Robin 1976].
71 Experiments have also shown rate-weakening is possible due to cavity formation behind hard bed
72 obstacles [Zoet & Iverson 2016] and pore-pressure feedback from clast ploughing [Thomason &
73 Iverson 2008]. Although each of these mechanisms, and the bed conditions which enable them,
74 show rate-weakening drag, their frictional evolution can differ dramatically. For example, the
75 critical slip distance (D_c) over which friction evolves to a new steady-state after a change in slip
76 rate varies by more than an order of magnitude between rock and till beds under similar conditions
77 in the same apparatus [McCarthy et al., 2017, Saltiel et al., 2021]. These mechanisms' different
78 frictional characteristics and applicable scales likely contribute to aspects of the resulting
79 seismicity, which could further constrain epicentral bed conditions.

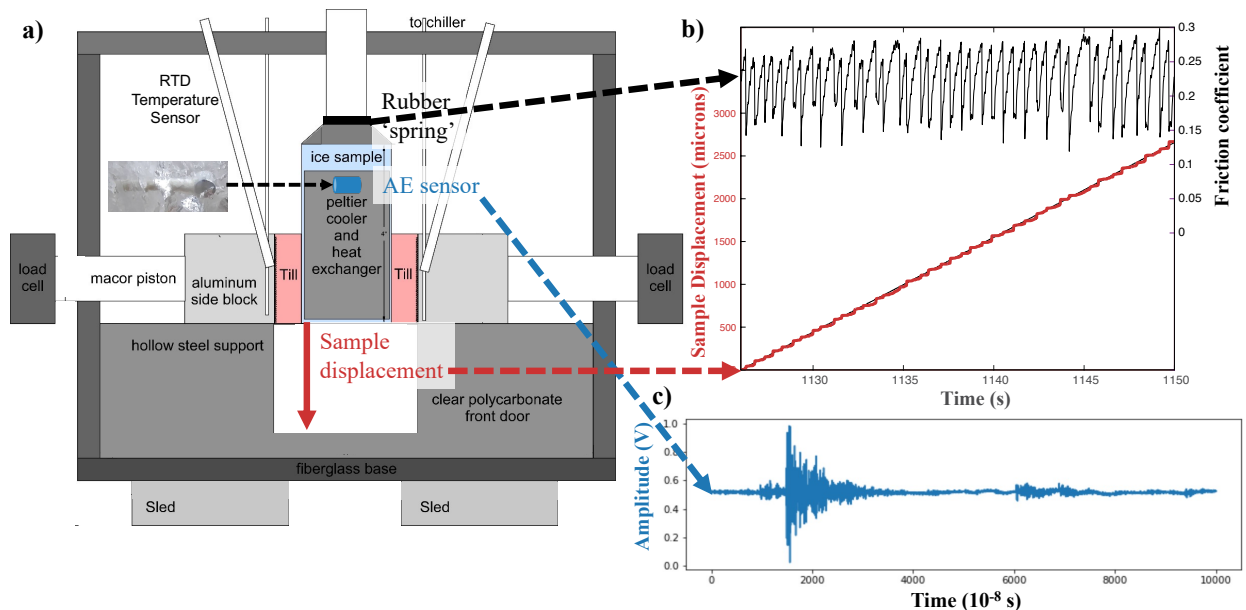
80 We report here, for the first time, experimental stick-slip stress-drops for pure ice on impermeable
81 rock and till at sub-freezing temperatures. In addition, we measured acoustic emissions (AEs) from
82 these settings and analyze the measured waveforms using machine learning (ML) classification
83 algorithms to find the characteristics associated with each bed type. By improving our
84 understanding of the mechanisms of unstable slip in glacial settings and their expression in seismic
85 emissions, these experiments and analysis techniques provide the opportunity to extract more
86 information on conditions / source mechanics of subglacial or other seismic settings.

87 **2 Experimental Methods and Materials**

88 Experiments were conducted using an ambient pressure, cryogenic temperature, servo-hydraulic
89 biaxial friction apparatus [McCarthy et al., 2016], with modifications to the insulating cryostat and
90 loading procedure to allow measurement of till [Saltiel et al., 2021]. In this double-direct-shear
91 configuration, a central ice block slides against two stationary side blocks, with layers of pre-
92 compacted and frozen till or rock on opposite sides of the ice, such that applied horizontal load is
93 resolved as normal stress and vertical load as shear stress on the sliding interfaces (Figure 1a).
94 Additional experimental details are described in supporting text S1.

95 We made three additional modifications to the apparatus from Saltiel et al., [2021]. A Linear
96 Variable Inductance Transducer (LVIT) position sensor measures the sample displacement
97 separate from the loading point's preset displacement. This allowed measurement of displacement
98 in each stress-drop 'slip' event as well as how much slip occurs during 'stuck' periods and the
99 timing of both relative to stress-drops (Figure 1b). Here we refer only to mechanical or bulk stress-
100 drops, the stress change during a slip event as measured by our vertical load cell, not to be confused
101 with seismologically derived stress-drops. A rubber material was inserted into the loading

102 geometry that effectively reduced the stiffness of the apparatus, reaching critical stiffness and
 103 allowing stick-slip instability [Zoet et al., 2020]. We estimate the effective apparatus stiffness
 104 using the mechanical data's reloading slope between stress-drops, relative to the compression of
 105 the loading train including rubber, the load point displacement minus sample displacement (Figure
 106 1b). We estimate the apparatus stiffness after adding the rubber to be $\sim 0.1 \text{ kPa}/\mu\text{m}$ or $\sim 5 \times 10^5$
 107 N/m , significantly less stiff than was estimated without the rubber $\sim 1 \text{ kPa}/\mu\text{m}$ [Saltiel et al., 2021].
 108 Additionally, commercial piezoelectric transducers were frozen into the central ice block, facing
 109 one of the ice-bed interfaces, to measure AEs. After experimenting with four different types of
 110 transducers of varying sizes and frequency sensitivities, we settled on Physical Acoustic's Nano-
 111 30™ miniature AE sensor due to its small size and 125-750 kHz response, covering the major
 112 frequency content of the events. All AEs analyzed here were recorded with a single Nano-30.



113 **Figure 1:** a) Schematic of biaxial cryostat with additions of rubber spring, to decrease loading
 114 stiffness, AE sensor frozen into central ice block (pictured within ice in inset on left), and sample
 115 displacement measurement, modified from Saltiel et al., [2021]. For more details about apparatus
 116 see that publication and supporting text S1. b) An example experiment of measured friction drops
 117 (in black on top) and stick-slip sample displacement (in red on the bottom) with the steady load
 118 point displacement (in black) for reference. Instability was induced by apparatus reaching
 119 subcritical stiffness. c) An example AE waveform before processing, from a single stress-drop.

121 AEs were recorded using a preamplifier and TiePie™ HS6 differential digital oscilloscope. To
 122 ensure we recorded all relevant spectral content in the waveforms, they were recorded at a sample
 123 rate of 100 MHz for 1 ms time windows around each event (Figure 1c). These oscilloscope settings
 124 provided the optimal real-time viewing of waveforms as they were being recorded (see supporting
 125 movie S1 of experiment including audible stress-drops), but subsequent analysis showed most of
 126 the energy was under 1 MHz, and waveforms were down-sampled to 10 MHz and windowed to
 127 15 μs . Recordings of continuous acoustic signal without applied shear found electrical noise above
 128 3 MHz, so filtering also helped remove persistent noise sources. The oscilloscope was set in rising-
 129 limb trigger mode with trigger amplitude set just above the noise level before slip initiates, such
 130 that it did not trigger without an audible stress-drop. Since electrical and other sources of noise
 131 can vary, this trigger level was adjusted throughout the experiment to maximize the number of

132 captured events and minimize waveforms of purely noise, but some events were missed, and some
133 events triggered by noise or other AE sources were saved.

134 **3 Data Processing and Machine Learning Analysis**

135 Most events directly correspond to bulk mechanical stress drops, but to remove AEs associated
136 with other types of sources (smaller patches of slip, cracking...), noisy events, non-events
137 triggered by noise, and to normalize the waveforms in a way that focuses on the initial wave
138 arrivals, we implemented a data cleaning and normalization approach based on that implemented
139 by Nolte & Pyrak-Nolte [2022], described in supporting text S2.

140 After removing noisy waveforms, we end up with 2817 total events, including 1547 waveforms
141 from 6 till experiments and 1270 waveforms from 6 rock experiments. With this labeled catalog
142 (Figure 2), we systematically explored the ability of numerous supervised ML algorithms to
143 predict the bed type for each event based on their waveform and spectra.

144 Input features to the machine learning models were the normalized waveform amplitudes at each
145 timestep or the \log_{10} power at each frequency for the spectra. The trained models select the most
146 important temporal portions of the waveforms or frequencies in the spectra for discriminating
147 between bed labels. We tested five basic ML classification algorithms including XGBoost (mean
148 prediction accuracy ~74%), random forests (~77%), support vector machines (~75%), Naïve
149 Bayes (~71%), K-nearest Neighbors (~76%), and fully connected neural networks (~75%). The
150 waveforms and spectra were independently broken into train and test datasets. Hyperparameters
151 were tuned for each algorithm and input data type (time or frequency domain) using 5-fold cross
152 validation, and the highest-accuracy model for each algorithm was then used for prediction on the
153 test set. The results of all our tests are summarized in supporting text S3, but here we focus our
154 analysis on the Random Forest Classifier model [Breiman 2001] applied to the processed catalog,
155 since it obtained some of our highest prediction accuracies, but, most importantly, it gives the
156 feature importance needed to interpret how the model obtains its results. The feature importance
157 shows the weighting of each waveform sample or frequency in making its prediction (Figures 4a
158 and b). The feature importance is key for interpreting how the prediction is made and visually
159 highlighting the subtle differences between different event sources. The purpose of this study is to
160 understand how bed differences manifest in the resulting emissions, not to find a black-box
161 algorithm which best differentiates them.

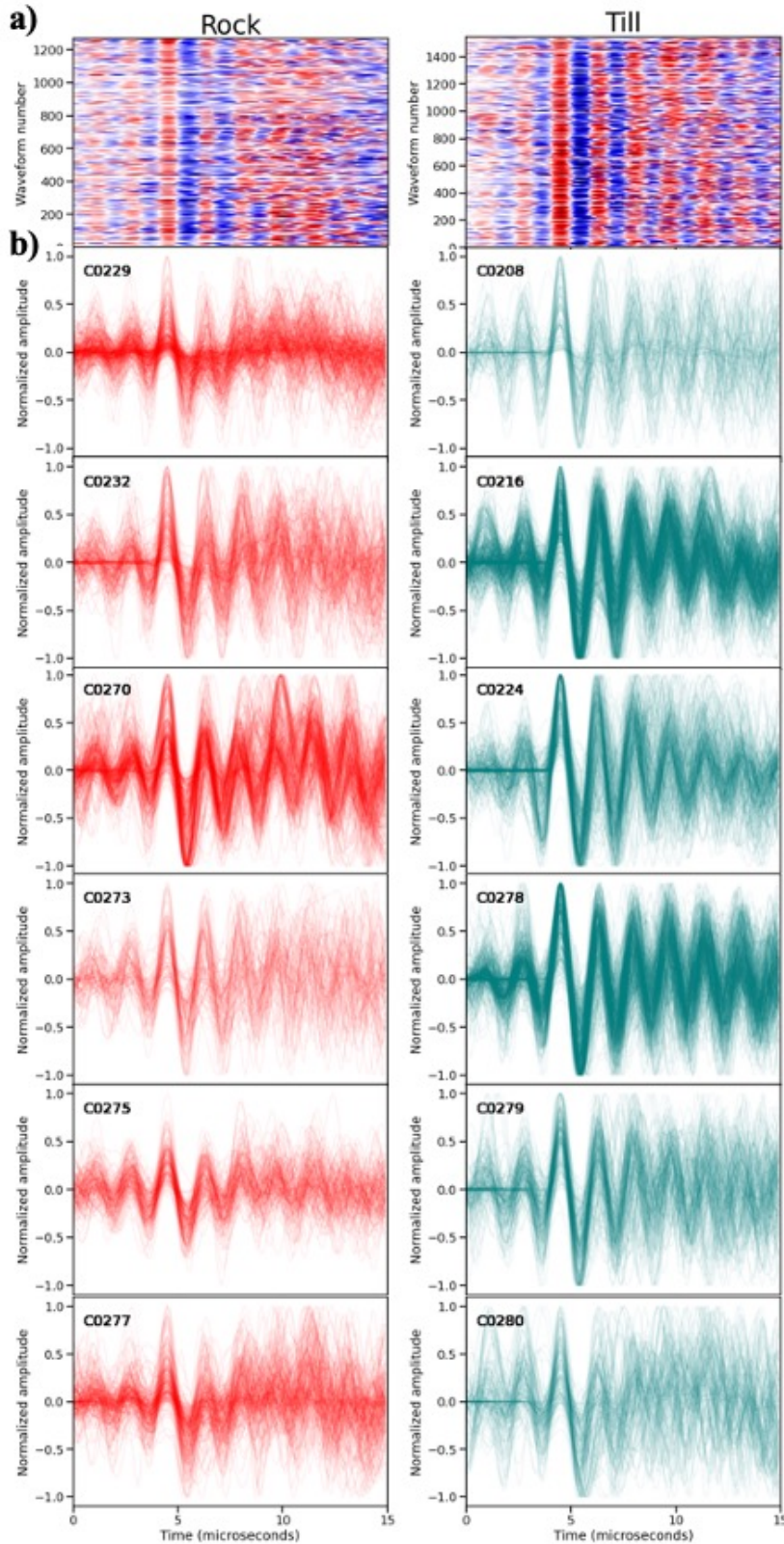
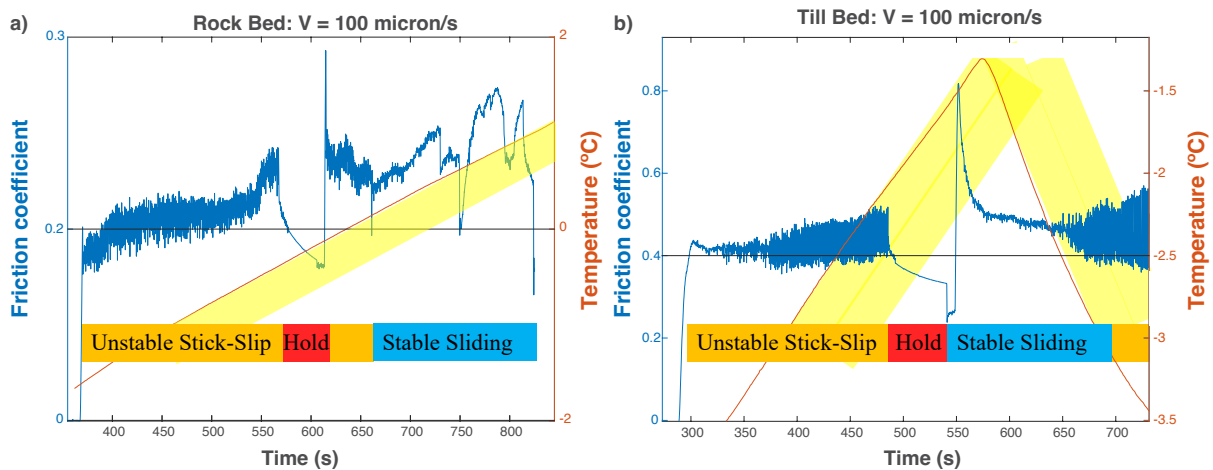


Figure 2: a) Waveforms plotted in chronological order along y-axis, colored by (normalized) amplitude (red is positive and blue negative). Rock events are plotted on the left and till on the right. b) Waveforms plotted together for each experiment (labelled on upper left). Each waveform (rock in red and till in teal) is plotted with a thin, light line, so the darker parts show many waveforms aligned on top of each other, and broader lines show less alignment. Since experiments vary significantly by number of events (94 – 465), that also contributes to the appearance of each experiment plot. Although there are subtle visual differences, it is not obvious that the two beds can be deciphered, making it a useful dataset to explore ML-based classification.

187 4 Stick-Slip Instability at Frozen Conditions

188 These experiments show the temperature dependence of instability, as both rock and till
 189 experiments were undertaken over a range of temperatures. Although analyzing the temperature
 190 dependence of AEs is outside of the scope of this letter, we did find stress-drops only at frozen
 191 temperatures ($< \sim 0$ °C for rock and $< \sim -2.5$ °C for till beds in Figure 3). It must be noted that
 192 temperatures are approximate, since they are measured behind the till/rock, there is some lag time
 193 before the temperature on the sliding interface reached those recorded. This is consistent with rate-
 194 weakening friction shown for till beds at ~ -3 °C using the same apparatus [Saltiel et al., 2021].
 195 We estimate the apparatus stiffness with rubber to be ~ 0.1 kPa/ μm or $\sim 5 \times 10^5$ N/m, which is the
 196 same order of magnitude as the critical stiffness estimated from velocity-step experiments ~ 0.02
 197 kPa/ μm or 1×10^5 N/m (calculation on page 13 of Saltiel et al., [2021]). This factor of five
 198 difference is consistent with the error inherit in applying estimations of rate-state friction
 199 parameters ($b - a$, D_c) from a single experiment, as well as in our rough estimation of apparatus
 200 stiffness. Past studies of ice on rock friction did not find rate-weakening until lower temperatures,
 201 $< \sim -18$ °C for McCarthy et al., [2017]. In that study, experiments above -18 °C which exhibited
 202 slight rate-strengthening were undertaken at less than half the slip rate, which could affect the rate-
 203 dependence as well as stability more broadly [Schulson & Fortt 2012]. It is also possible to reach
 204 instability at nominally stable conditions given the strong elastic contrast between ice and rock
 205 beds [Rice et al., 2001]. This highlights the range of factors that contribute to seismic instability,
 206 further experiments and analysis are needed to fully map the conditional dependence of stability.



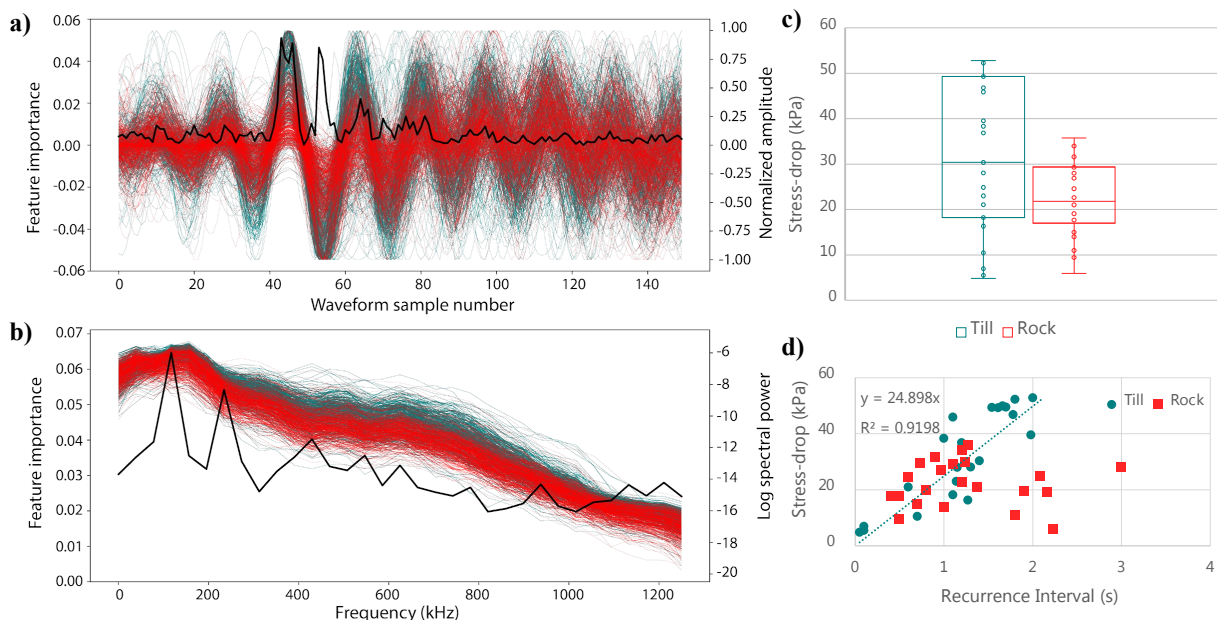
207 **Figure 3:** Example experiments of the temperature effect on slip stability for **a)** rock and **b)** till
 208 beds. Each experiment begins with stress-drops but, after a hold (described in supporting text S1),
 209 with increasing temperature the ice starts to slide stably without sudden friction drops or audible
 210 stick-slips. The transition to stable sliding occurs around 0 °C for the rock experiment. In the till
 211 experiment, the stability temperature is reached during the hold, but as it is re-cooled stress-drops
 212 resume below about -2.5 °C. Each estimated transition temperature is highlighted with a solid
 213 black horizontal line, but the temperatures are not measured directly at the ice-bed interface, so the
 214 interface temperature lags that recorded. The lag time (estimated to be ~ 100 s given rock/till
 215 thermal diffusivities ~ 1 mm²/s) is represented by the yellow region right of the measured
 216 temperature. Additionally, when the temperature probe goes above ~ 0 °C the ice will remain at its
 217

218 pressure melting point. It is also apparent that the till experiment has higher friction and healing
 219 rate (as the friction rose more after hold times of similar duration).

220 5 Bed Type Classification from Acoustic Emissions

221 Using a wide range of classification algorithms, we consistently find prediction accuracy above
 222 50%, mostly between 65% and 80% (Supporting Figure S3), showing it is possible to tell if a
 223 population of AEs was emitted by a till or rock bed. This is not clear by visually examining the
 224 waveforms (Figure 2), showing algorithms successfully extract subtle features corresponding to
 225 the different bed labels. The logarithm of event spectra is also predictive (see supporting text S4).

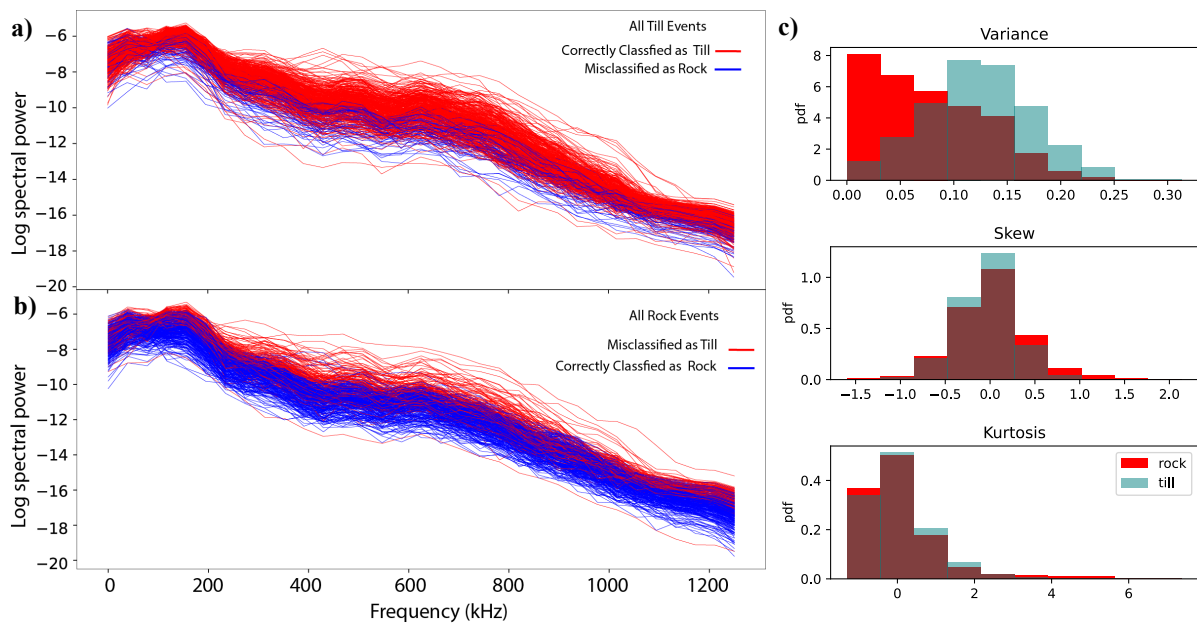
226 To be able to apply our findings from laboratory AEs to field-scale seismicity, it is vital that we
 227 can interpret how the algorithms make their prediction. Although transfer learning methods offer
 228 the potential to train with labelled laboratory or modelled datasets and ‘transfer’ the model to more
 229 limited field or laboratory data [e.g., Wang et al., 2021], clear differences in the spectral content,
 230 travel path effects, and scale of field seismic data make this a daunting task. By isolating and
 231 interpreting the features the algorithms are using to make their successful predictions, we can
 232 understand the differences to look for and interpret in field data. The feature importance for the
 233 Random Forest Classifier model shows that it focuses on the peak and valley of the first full
 234 oscillation of the initial wave arrival (Figure 4a). Plotting all the normalized waveforms (color
 235 coded by bed type) together, we can see that the till (teal) waves tend to have higher amplitude in
 236 these first peaks. Similarly, log spectra show more energy at higher frequencies for the till in
 237 comparison to rock spectra (Figure 4b). Analyzing the mechanical data from 23 till and 22 rock
 238 experiments (including other experiments without recorded AEs), we find that the stress-drops of
 239 stick-slip events on till beds are generally higher (Figure 4c). The more impulsive arrivals and
 240 higher frequency content is consistent with till’s higher stress-drops, since seismological stress-
 241 drop is calculated by the corner frequency where energy starts to fall off [e.g., Zoet et al., 2012].
 242 This, in turn, can be explained by till’s higher healing (Figures 3 and 4d), friction (Figure 3), as
 243 well as the rougher till surface (with its larger grain sizes).



244 **Figure 4:** a) Feature importance, showing the weighting of each waveform sample to the model
 245 prediction, highlights the importance of the initial wave arrivals. The superimposed normalized
 246

247 waveforms show till (teal) events are higher amplitude than rock (red) in these first oscillations.
 248 **b)** Feature importance of each frequency in the model prediction, show till (teal) and rock (red)
 249 spectra partially separate from each other above about 100 kHz, with till having more energy at
 250 these higher frequencies. **c)** Distribution of largest repeated mechanical stress-drop amplitude from
 251 23 till and 22 rock experiments at similar conditions show till has higher stress-drops, although the
 252 two populations overlap significantly. **d)** Stress-drops vs recurrence interval for till and rock
 253 experiments shows till's greater healing (higher slope) contributes to higher stress-drops, while
 254 rock healing varies, but is generally lower.

255 It is likely that obtaining much higher prediction accuracies is impossible since each bed creates
 256 events like the other. The stress-drop and healing rates of the two populations clearly overlap
 257 (Figure 4c and d); spectra and waveform characteristics do as well. How this effects prediction can
 258 be most clearly seen with the log spectra since the visual separation is greatest. Figure 5a and b
 259 show that misclassified events are in the region between the event types, while Figure 5c shows
 260 that the waveform statistical attributes also greatly overlap. Although correctly predicting every
 261 event is unrealistic, given a sufficient sample size, our results suggest it could be possible to predict
 262 the bed type of a group of events from the same epicentral conditions (see supporting text S5).



263 **Figure 5:** Log spectra of correct and misclassified **a)** till and **b)** rock events and **c)** distributions of
 264 statistical measures of waveforms from all experiments from each bed show how much the event
 265 populations overlap. The higher variance in the till waveform distributions is due to their more
 266 impulsive nature, but there are many rock events with just as high variance.
 267

268 6 Conclusions

269 This study presents stick-slip stress-drops and resultant AEs for ice on rock and till beds at sub-
 270 freezing temperatures, a labeled dataset with which we explore how ML can decipher the bed from
 271 AE characteristics. We found that instability, and thus seismicity, only occurs for each bed below
 272 a certain temperature (~ 0 °C for rock and ~ -2.5 °C for till), sliding stably as the temperature warms
 273 above and stick-slipping again when frozen below these estimated temperatures. Although the
 274 different bed types exhibit stick-slip behaviors at similar conditions, the mechanics of their drag

275 are very different, demonstrated by friction that evolves over an order of magnitude more distance
276 (D_c), significantly more rate-weakening ($b - a$), higher friction, and healing rates in frozen till
277 compared to rock beds [Saltiel et al., 2021]. Resultant emissions have subtle differences, difficult
278 to decipher visually, but which ML-based classification was able to identify; successfully
279 predicting the bed type of a given waveform about 65% to 80% of the time, depending on the
280 classification algorithm, processing steps, and data type used. The Random Forest Classifier was
281 particularly successful (~77% mean prediction accuracy) and interpretable, since it provides
282 feature importance of each waveform sample or frequency, showing the models focus on the initial
283 wave arrivals and certain frequencies, where till events are higher amplitude. This is consistent
284 with till's more impulsive failure, higher stress-drops, and friction, in turn due to a rougher and
285 faster healing interface.

286 Given how different the slip mechanics of these two beds are, it is somewhat surprising how similar
287 the resultant AEs are, but the interpretability of our ML results offers a path forward for
288 classification. The findings are also counter to our original hypothesis based on the much longer
289 frictional evolution distances (D_c) found in velocity-step experiments, which suggest less
290 impulsive, lower frequency emissions. It is likely that different aspects of the frictional mechanics
291 counter each other, for example more healing has been associated with higher frequency emissions
292 in laboratory and natural faults [McLaskey et al., 2012], which could cancel the spectral effect of
293 longer D_c . In a similar way, till experiments' higher D_c and $b - a$ balance each other to produce a
294 critical rheological stiffness of the same order as rock [Saltiel et al., 2021]. In the end, our findings
295 suggest that supervised ML-based classification and unsupervised correlation studies could find
296 unknown and non-intuitive relationships between seismic emission characteristics and the
297 mechanics / conditions of rupture in subglacial, as well as tectonic, volcanic, or induced seismicity
298 settings. Laboratory experiments offer the opportunity to obtain well-controlled, labeled datasets,
299 but results need to be interpretable. Although it will be difficult to transfer models trained in the lab
300 directly to field-scale data, the understanding gained can be used to infer characteristics of natural
301 seismic sources.

302 **Acknowledgments, Samples, and Data**

303 S. Saltiel acknowledges the support of the Lamont-Doherty Postdoctoral Fellowship in Earth and
304 Environmental Sciences. This research and S. Saltiel and C. McCarthy were funded by National
305 Science Foundation (NSF)-1854629. Many thanks to T. Mittal for data processing and ML analysis
306 suggestions, J. Tielke and T. Koczyński for laboratory assistance, as well as C. Marone, J. Rivière,
307 and the Penn State Rock and Sediment Mechanics Lab for experimental acoustics advice.

308 **Open Research**

309 The datasets generated for this study are available on figshare.com at doi:
310 [10.6084/m9.figshare.21257730](https://doi.org/10.6084/m9.figshare.21257730), and Jupyter notebook for processing data is available at
311 <https://github.com/StraboAI/IcesAEs>.

312 **References**

- 313 Aster, R. C., & Winberry, J. P. 2017. Glacial seismology. *Reports on Progress in Physics*, **80**,
314 126801. doi:10.1088/1361-6633/aa8473
- 315 Bougamont, M., Christoffersen, P., Price, S. F., Fricker, H. A., Tulaczyk, S., & Carter, S. P.
316 2015. Reactivation of Kamb Ice Stream tributaries triggers century-scale reorganization

- 317 of Siple Coast ice flow in West Antarctica. *Geophysical Research Letters*, **42**(20), 8471-
318 8480.
- 319 Breiman, L. 2001. Random Forests. *Machine Learning* **45**, 5–32 doi:10.1023/A:1010933404324
- 320 Clarke, G. K. 2005. Subglacial processes. *Annual Review of Earth and Planetary Sciences*, **33**(1),
321 247-276.
- 322 Cole, D. M. 1979. Preparation of polycrystalline ice specimens for laboratory experiments, *Cold*
323 *Reg. Sci. Technol.*, 1, 153–159, doi: 10.1016/0165-232X(79)90007-7.
- 324 Cuffey, K.M. & Paterson, W.S.B., 2010. *The Physics of Glaciers*, 4th ed, Elsevier
- 325 Gräff, D., Köpfli, M., Lipovsky, B. P., Selvadurai, P. A., Farinotti, D., & Walter, F., 2021. Fine
326 structure of microseismic glacial stick-slip. *Geophysical Research Letters*, **48**,
327 e2021GL096043. <https://doi.org/10.1029/2021GL096043>
- 328 Gräff, D., & Walter, F., 2021. Changing friction at the base of an Alpine glacier. *Sci. Rep.* **11**,
329 10872. <https://doi.org/10.1038/s41598-021-90176-9>
- 330 Guerin, G., Mordret, A., Rivet, D., Lipovsky, B. P., & Minchew, B. M., 2021. Frictional origin of
331 slip events of the Whillans Ice Stream, Antarctica. *Geophysical Research Letters*, **48**(11),
332 e2021GL092950.
- 333 Iverson, N.R., 2010. Shear resistance and continuity of subglacial till: hydrology rules. *Journal of*
334 *Glaciology*, **56** (200) 1104-1114. doi:10.3189/002214311796406220.
- 335 Hudson, T., Kufner, S. K., Brisbourne, A., Kendall, M., Smith, A., Alley, R., ... & Murray, T.
336 2022. Friction and slip measured at the bed of an Antarctic ice stream., Preprint from
337 *Research Square*, DOI: 10.21203/rs.3.rs-1214097/v1
- 338 Kufner, S.-K., Brisbourne, A. M., Smith, A. M., Hudson, T. S., Murray, T., Schlegel, R., et al.
339 2021. Not all icequakes are created equal: Basal icequakes suggest diverse bed deformation
340 mechanisms at Rutford Ice Stream, West Antarctica. *Journal of Geophysical Research:*
341 *Earth Surface*, 126, e2020JF006001. Doi:10.1029/2020JF006001
- 342 Lipovsky, B.P., Meyer, C.R., Zoet, L.K., McCarthy, C., Hansen, D.D., Rempel, A.W. & Gimbert,
343 F., 2019. Glacier sliding, seismicity and sediment entrainment. *Annals of Glaciology*,
344 **60**(79), pp.182-192.
- 345 Marone, C., 1998. Laboratory-derived friction laws and their application to seismic faulting, *Ann.*
346 *Rev. Earth Planet. Sci.*, **26**, 1, 643–696.
- 347 McCarthy, C., Savage, H.M., Koczyński, T., & Nielson, M.A., 2016. An apparatus to measure
348 frictional, anelastic, and viscous behavior in ice at temperate and planetary conditions.
349 *Review of Scientific Instruments*, **87**.
- 350 McCarthy, C., Savage, H.M., & Nettles, M., 2017. Temperature dependence of ice-on-rock friction
351 at realistic glacier conditions, *Phil. Trans. R. Soc. A*, **375** (2086), 20150348.
- 352 McLaskey, G. C., Thomas, A. M., Glaser, S. D., & Nadeau, R. M., 2012. Fault healing promotes
353 high-frequency earthquakes in laboratory experiments and on natural faults. *Nature*,
354 **491**(7422), 101-104.
- 355 Nolte, D. D., & Pyrak-Nolte, L. J., 2022. Monitoring fracture saturation with internal seismic
356 sources and twin neural networks. *Journal of Geophysical Research: Solid Earth*, **127**(2),
357 e2021JB023005.
- 358 Parizek, B. R., Christianson, K., Anandakrishnan, S., Alley, R. B., Walker, R. T., Edwards, R. A.,
359 Wolfe, D. S., Bertini, G. T., Rinehart, S.K., Bindschandler, R. A., & Nowicki, S. M. J.,
360 2013. Dynamic (in) stability of Thwaites Glacier, West Antarctica. *Journal of Geophysical*
361 *Research: Earth Surface*, **118**(2), 638-655.

- 362 Rice, J. R., N. Lapusta, & Ranjith K., 2001. Rate and state dependent friction and the stability of
363 sliding between elastically deformable solids, *J. Mech. Phys. Solids*, **49**, no. 9, 1865–1898.
- 364 Robin, G. de.Q. 1976. Is the Basal Ice of a Temperate Glacier at the Pressure Melting Point?
365 *Journal of Glaciology*, **16**(74), 183-196. doi:10.3189/S002214300003152X.
- 366 Saltiel, S., McCarthy, C., Creyts, T. T., & Savage, H. M., 2021. Experimental evidence of velocity-
367 weakening friction during ice slip over frozen till: Implications for basal seismicity in fast
368 moving, soft-bed glaciers and ice streams. *Seismological Research Letters*, **92**(5), 2793-
369 2810.
- 370 Schoof, C. 2005. The effect of cavitation on glacier sliding. *Proceedings of the Royal Society A:*
371 *Mathematical, Physical and Engineering Sciences*. 461.2055. 609-627.
- 372 Schulson, E. M., & Fortt, A. L. 2012. Friction of ice on ice. *Journal of Geophysical Research:*
373 *Solid Earth*, **117**(B12).
- 374 Thomason, J.F. & Iverson, N.R., 2008. A laboratory study of particle ploughing and pore-pressure
375 feedback: a velocity-weakening mechanism for soft glacier beds. *Journal of Glaciology*,
376 **54**(184), pp.169-181.
- 377 Wang, K., Johnson, C. W., Bennett, K. C., & Johnson, P. A., 2021. Predicting fault slip via transfer
378 learning. *Nature communications*, **12**(1), 1-11. Doi: 10.1038/s41467-021-27553-5
- 379 Zoet, L. K., Anandakrishnan, S., Alley, R. B., Nyblade, A. A. & Wiens, D. A., 2012. Motion of an
380 Antarctic glacier by repeated tidally modulated earthquakes. *Nature Geoscience*, **5**, 623-
381 626.
- 382 Zoet, L.K., Carpenter, B., Scuderi, M., Alley, R.B., Anandakrishnan, S., Marone, C., Jackson, M.,
383 2013. The effects of entrained debris on the basal sliding stability of a glacier. *Journal of*
384 *Geophysical Research: Earth Surface*, **118**, 656-666.
- 385 Zoet, L.K., & Iverson, N.R., 2016. Rate-weakening drag during glacier sliding. *Journal of*
386 *Geophysical Research: Earth Surface*, **121**(7), 1206-1217.
- 387 Zoet, L.K. & Iverson, N.R., 2018. A healing mechanism for stick-slip of glaciers. *Geology*, **46**(9),
388 pp.807-810.
- 389 Zoet, L.K. & Iverson, N.R., 2020. A slip law for glaciers on deformable beds. *Science*, **368**(6486),
390 pp.76-78.
- 391 Zoet, L.K., Ikari, M.J., Alley, R.B., Marone, C., Anandakrishnan, S., Carpenter, B.M., & Scuderi,
392 M.M., 2020. Application of constitutive friction laws to glacier seismicity. *Geophysical*
393 *Research Letters*, **47**(21), e2020GL088964.